3D numerical modelling of graben interaction and linkage: a case study of the Canyonlands grabens, Utah

Vaneeda Allken, Ritske S. Huismans, Haakon Fossen and Cedric Thieulot
Department of Earth Sciences, University of Bergen, Bergen, Norway

ABSTRACT

Graben systems in extensional settings tend to be segmented with evidence of segment interaction. To gain a better understanding of the evolution of structures formed during graben growth and interaction, we here study the Grabens area of Canyonlands National Park, Utah, where a wide range of such structures is well exposed. With the aid of 3D numerical models, we attempt to reproduce structures observed in that region and to understand controls on the structural style of graben interaction by varying the spacing between pre-existing structures. The sensitivity of the system to the thickness of the salt layer is also tested. Four distinct types of structures are observed when the spacing between inherited weak zones is varied: (1) grabens connecting in a relay zone divided by a narrow central horst; (2) graben segments interacting via a secondary stepover graben; (3) grabens propagating alongside each other with limited segment interaction; and (4) an abandoned graben segment in a system of multiple competing grabens. The presence of a basal salt layer (Paradox Member) promotes efficient graben propagation. A comparison between the observed structures and the numerical model results indicates that the detachment salt layer is relatively thin in the study area.

INTRODUCTION

Fault interaction is a well-known phenomenon that occurs in any tectonic setting where fault populations evolve, and has received much attention in extensional systems. The understanding of this process has significant implications for the way we understand fault growth in general and structurally complex hydrocarbon reservoirs in particular (e.g., Morley, 1999; Cowie *et al.*, 2000; Jackson *et al.*, 2002; Morewood & Roberts, 2002). A particularly interesting feature of almost any rift system is segmented graben systems and the way that individual graben segments interact. Graben segmentation and segment interaction are commonly seen in many grabens of rift systems, such as the Viking Graben of the North Sea (e.g., Fossen *et al.*, 2010), but may also occur at a smaller scale within populations of extensional faults. The Grabens area in the Needles District of Canyonlands National Park, Utah is an example where multiple well-exposed grabens evolved by segment growth and interaction (Trudgill & Cartwright, 1994). The geometries and patterns of graben linkage that are observed in this and similar areas call for a better understanding of controlling parameters, such as pre-existing weakness, the significance of an underlying décollement, offset of initial gra-

ben segments and the role of material properties. In an attempt to address the role of some of these parameters, we have conducted a series of 3D numerical modelling experiments by means of a finite element code that allows for the formation and interaction of frictional-plastic shear zones and graben segments. This work adds to previous 2D modelling of this graben system by Schultz-Ela & Walsh (2002), who pointed out the need for further examination of factors controlling the 3D structural style of graben propagation and linkage. The numerical models presented here add to the more general and larger scale models presented in a complementary article (Allken *et al.*, 2011), which showed that structures similar to those observed in the Canyonlands region could be reproduced with a single rigid–plastic material. The presence of an underlying ductile layer was subsequently shown to have a significant effect on graben interaction (Allken *et al.*, 2012). In the Canyonlands region, in particular, the presence of an underlying salt layer is generally acknowledged to be necessary for extension and faulting (e.g., Baker, 1933; McGill & Stromquist, 1979; Huntoon, 1982). But its exact role on the formation of the Grabens has not been determined (Schultz-Ela & Walsh, 2002). The fact that a salt layer underlies the Canyonlands fault population is therefore taken into account in the models presented in this article. Particular attention is paid to the formation of a narrow horst observed in some of the Canyonlands grabens, the style of graben interaction and the control of graben segment spacing (lateral offset of graben axes) and length of pre-existing weak structures. Finally, the sensitivity of the system to the thickness of

Correspondence: Vaneeda Allken, Department of Earth Sciences, University of Bergen, Allégaten 41, 5007 Bergen, Norway. E-mail: vaneeda@gmail.com
Present address: Institute of Earth Sciences, Utrecht University, Utrecht, the Netherlands

the salt layer is tested and implications for salt thickness are investigated.

CANYONLANDS

Geological setting

The Grabens area in the Needles District of Canyonlands National Park is situated on the south-east side of the Colorado River on the Colorado Plateau, immediately south of the confluence of the Green and the Colorado river (Fig. 1). Located south-west of the Paradox fold and thrust belt, the southern Canyonlands region as a whole is only very mildly deformed, with very gentle upright folds related to the Laramide orogeny farther east. Salt walls and related structures found in the Moab areas to the north (Trudgill, 2011) are absent owing to the thin Pennsylvanian salt layer(s) in this area (Barbeau, 2003). In this general setting, the Grabens area and its arcuate array of steep normal faults stand out as a structural anomaly (McGill & Stromquist, 1979). The faults, which show offsets of up to 150–200 m, are well exposed at the surface, and bound grabens that are 100–400 m wide, with an average width of 250 m (Trudgill, 2002). We assume the
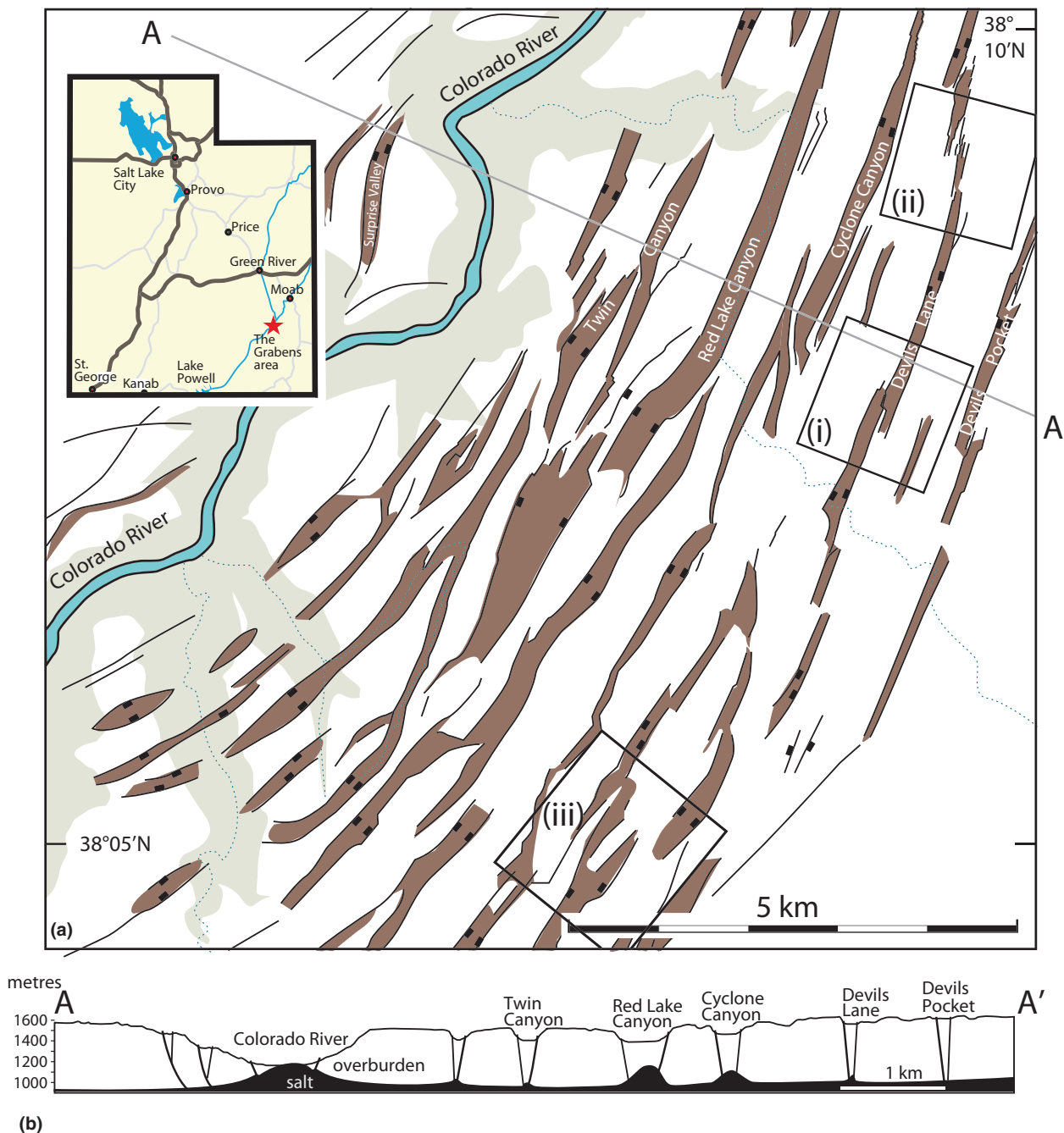

Fig. 1. (a) Structural map showing the population of grabens in the Grabens area in Canyonlands National Park, Utah and (b) cross-section of the Graben area, partly based on Schultz-Ela & Walsh (2002). Some selected examples (i, ii, iii) are shown in 3D in Fig. 9.

faults extend through the 400–450 m thick succession of Permian sandstone and limestone decoupling in the evaporate deposits of the Paradox Member of the Pennsylvanian Hermosa Formation. The Paradox Formation is comprised of multiple evaporite sequences and therefore, multiple halite layers that could form a detachment layer. The sandstone and limestone package is crosscut by a densely spaced vertical joint system (e.g. Fig. 4 in Moore & Schultz, 1999). The grabens are aligned parallel to one of the two regional joint sets, although graben-bounding faults locally cut across this set of pre-existing fractures. The faults are close to vertical at the surface, but deep drainage exposures indicate that they flatten to 70–75º at *ca.* 200 m below the surface (McGill & Stromquist, 1979; Trudgill & Cartwright, 1994; McGill *et al.*, 2000).

Mechanics of graben formation

The occurrence of the extensional fault array in the Grabens area is related to late Quaternary gravitational sliding of the brittle sandstones and limestones on top of viscously deforming salt of the Paradox Member (McGill & Stromquist, 1979). Gravitational sliding is facilitated by a regional 2–4º dip towards the north-west (Huntoon, 1982), and it is assumed that the translations started when erosion by the Colorado River exposed the salt of the Paradox Member (McGill *et al.*, 2000), within the last 0.5 Ma (Trudgill, 2002). The young age of the grabens is also demonstrated by dramatic changes in stream drainage patterns (Trudgill, 2002), and current westward translation of the Graben area is demonstrated by Furuya *et al.* (2007) based on analysis of InSAR data. The grabens appear to be less mature and hence younger to the southeast (Trudgill, 2002), suggesting that the brittle supra-salt sequence failed successively from the Colorado River canyon and up-dip. In addition, InSAR mapping suggests more rapid strain accumulation across the faults closer to the eastern edge of the array. Dating of sediments in the grabens supports this interpretation (Biggar & Adams,

1987; Trudgill, 2002). More importantly, the grabens are segmented with the formation of double sets of relay ramps at the segment boundaries (Trudgill & Cartwright, 1994). The offset of the graben axis varies from half the width of the graben up to several times the graben width. In the latter case, short (100–1000 m long) graben segments form between the major (several km-long) grabens. While the specific geometries of the grabens are strongly influenced by the strength anisotropy associated with the pre-existing joint set (Moore & Schultz, 1999), they are believed to have initiated at the base of the brittle layer and propagated both upwards and laterally within the brittle plate (McGill & Stromquist, 1979). Some studies, however, oppose this view and suggest that they may have propagated downwards (Melosh & William, 1989; Walsh & Schultz-Ela, 2003). The segmented nature of the grabens is interpreted as occurring by linkage of segments as the faults grow laterally (Cartwright *et al.*, 1995; Cartwright & Mansfield, 1998; Cowie *et al.*, 2000). Several stages of interaction can be observed, but cases where fault breaching occurs early in the linkage process are particularly well-exposed.

NUMERICAL MODELLING APPROACH

To model the evolution and interaction of graben structures for a system, such as the Canyonlands region, which is driven by extension, we used a three dimensional Arbitrary Lagrangian Eulerian (ALE) fully parallel Finite Element code (Thieulot, 2011). This code solves the Stokes equation for three-dimensional visco-plastic flows with large deformation.

Rheology

In the continuum mechanics context, brittle failure is approximated by viscous deformation following a plastic yield criterion. The rheological behaviour of the Permian
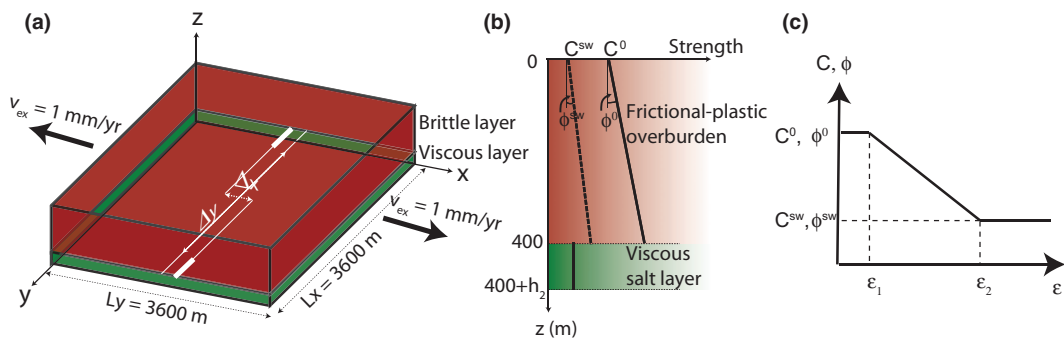

Fig. 2. (a) Model setup representing an area of 3600 m × 3600 m where a frictional-plastic sediment layer of thickness 400 m overlies a viscous salt layer of thickness h_2. Two weak seeds are placed at the base of the frictional-plastic layer at an offset Δ_x and with an underlap Δ_y. Extensional boundary conditions of 1 mm year^{-1} are applied on two opposite sides of the box. (b) Rheological profile implemented: Mohr-Coulomb plasticity (initial + strain-weakened) in the sediment layer and a linear Newtonian viscosity, μ_2 in the salt layer. (c) Frictional plastic strain weakening behaviour of the brittle upper layer. For $\varepsilon < 0.25$, the cohesion, C and angle of friction, ϕ are constant at 2.50 MPa and 30º. When $0.25 < \varepsilon < 1.25$, the material strain weakens, i.e. C and ϕ decrease linearly from 2.50 MPa to 0.75 MPa and 30º to 25º. Beyond $\varepsilon = 1.25$, C and ϕ remain constant at 0.75 MPa and 25º.

sedimentary succession (overburden) is approximated with the pressure-dependent frictional–plastic Mohr-Coulomb yield criterion (Ranalli, 1995), where the plastic yield stress σ_y is a function of pressure, the internal angle of friction, ϕ and the cohesion C:

$$\sigma_y = C cos(\varphi) + P sin(\varphi) \quad (1)$$

C and ϕ are both functions of the accumulated strain (Fig. 2c). ε_1 denotes the lower strain-weakening threshold at which strain-weakening starts while the upper strain weakening threshold at which the material reaches full strain-weakened value is denoted by ε_2. For $\varepsilon \leq \varepsilon_1$, C and ϕ are set to C_0 and ϕ_0 respectively. When the strain in a cell reaches ε_1, the material starts to strain weaken, i.e., the cohesion C and the angle of friction ϕ decrease linearly with strain until a final strain weakened value (C_{sw}, ϕ_{sw}) is reached at $\varepsilon = \varepsilon_2$. A salt detachment in one of the halite layers of the Paradox formation is approximated with a linear Newtonian viscous flow law with a constant viscosity, μ_2 (Fig.2b).

Model geometry

The model domain, of size $L_x \times L_y \times L_z$, consists of a frictional–plastic material of density ρ_1 (overburden) overlying a viscous salt layer of density ρ_2 (Fig. 2a). The faulted Permian overburden layer is characterized by its initial and final cohesion, C_0 and C_{sw}, and initial and final angle of friction, ϕ_0 and ϕ_{sw} as well as its strain weakening parameters, ε_1 and ε_2, while the salt layer is characterized by its dynamic viscosity μ_2 (Fig. 2b). To initiate the localization of deformation, two weak seeds, each with a cross-section of 50 m $\times$ 25 m (the length of the weak seed along the *y*-axis varies throughout the experiments), are placed at the base of the overburden (Fig. 2a) as the model is expected to be most sensitive to perturbation in strength at depth, rather than close to the surface. In those regions, strain is set to strain-weakened values at the beginning of the experiments. The system is extended

orthogonally with the following boundary conditions: free slip on faces y = 0, y = L_y and at the bottom of the model domain (z = 0), imposed extensional velocities, v_{ext}, on faces x = 0 and x = L_x, and a free surface at the top of the model domain. There is no movement in the y-direction. In our models, both the frictional–plastic and the viscous layer are extended at a constant velocity.

Choice of parameters

To best reproduce conditions matching those found in the Canyonlands region, the values presented in Table 1 were used for the models. Rock properties are not very well-known in this region. It has been shown empirically that at shallow depths, cohesion tends to zero and the angle of internal friction is around 40º (Byerlee, 1978). In the Grabens area, the effective cohesive strength of the rocks has been estimated to be less than 5 MPa (McGill & Stromquist, 1979). In all models the initial cohesion is set to 2.5 MPa. The choice for the angle of friction (initial and strain weakened) was based on previous 2D modelling work (Schultz-Ela & Walsh, 2002) in the Grabens area, which indicates that the most realistic fault patterns were obtained around these values.

Model limitations

(1) The computational intensity required for these three-dimensional models limits the numerical model resolution. The computational grid used was composed of $144 \times 144 \times 18 = 373,248$ elements, which results in a spatial mesh resolution of 25 m.
(2) We assume the material to be incompressible and use a non-associated plastic flow law, which means that dilation is not taken into account in our models. Plastic shear zones in these conditions form approximately at 50–55º, tending towards Arthur angles (52.5º here), as predicted by Kaus (2010) for low numerical resolution.

Table 1. Value of model parameters used

Symbol	Meaning	Value
L_x	Length of model along *x*-axis	3600 m
L_y	Length of model along *y*-axis	3600 m
h_1	Thickness of overburden	400 m
h_2	Thickness of salt detachment	50, 75, 100 m
ρ_1	Density of overburden	2400 kg m^{-3}
ρ_2	Density of salt layer	2200 kg m^{-3}
μ_2	Viscosity of salt layer	10^{17} Pa s
g	Acceleration due to gravity	9.81 m s^{-2}
C^0	Initial cohesion	2.50 MPa
C^{sw}	Final strain-weakened cohesion	0.75 MPa
ϕ^0	Initial angle of friction	30
ϕ^{sw}	Strain-weakened angle of friction	25
ε_1	Strain weakening threshold	0.25
ε_2	Onset of full strain weakened state	1.25
v_{ext}	Extensional velocity	1 mm year^{-1}

Table 2. Values used for the offset Δ_x, the underlap, Δ_y and the thickness h_2 of the salt layer in models 1–15

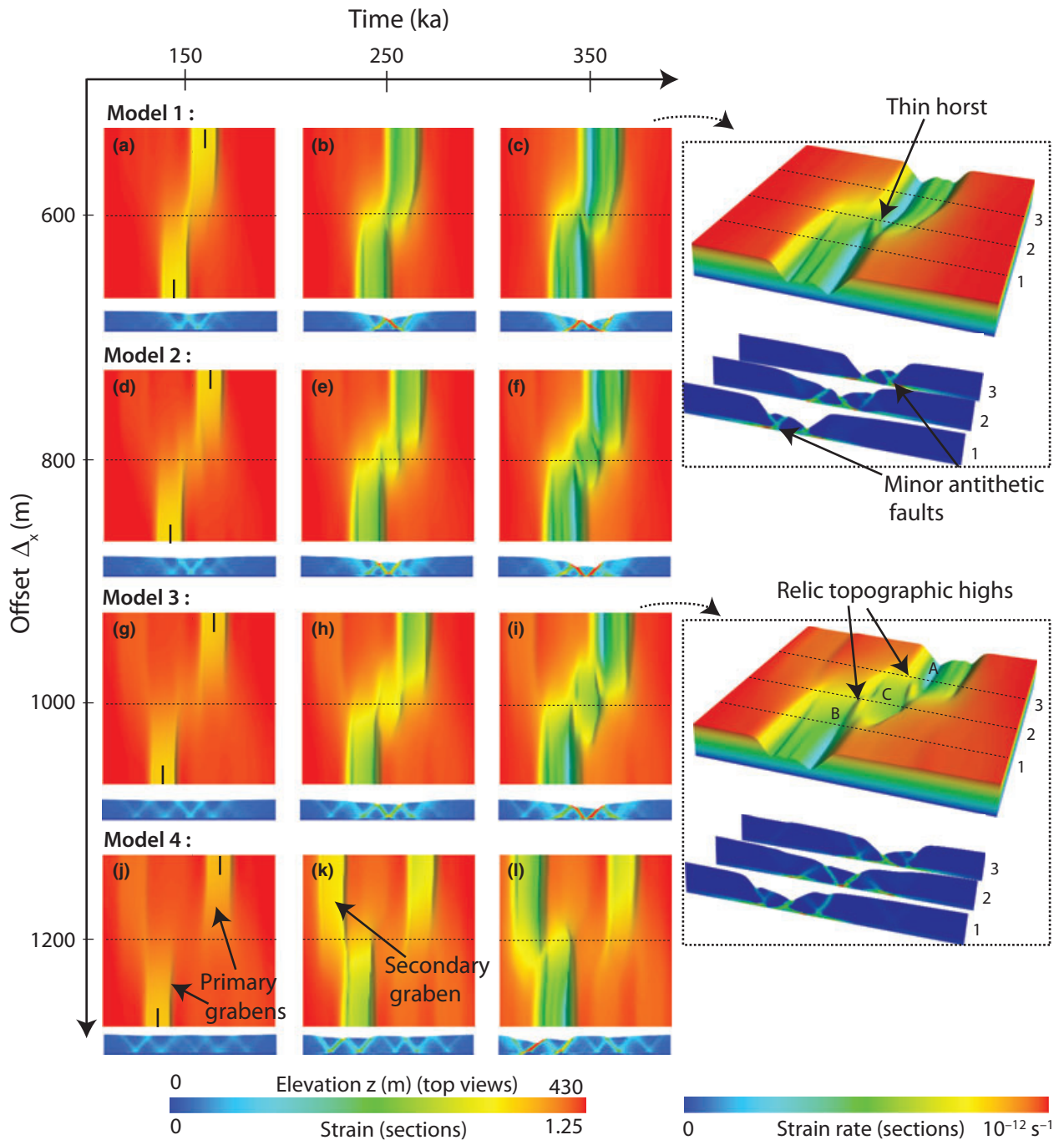| Model no	Δ_x (m)	Δ_y (m)	h_2 (m)	Figure no
1	600	2800	50	3, 6, 8
2	800	2800	50	3
3	1000	2800	50	3, 7, 8
4	1200	2800	50	3, 8
5	600	1800	50	4, 8
6	800	1800	50	4
7	1000	1800	50	4, 8
8	1200	1800	50	4, 8
9	600	−200	50	5, 8
10	1000	−200	50	5, 8
11	1200	−200	50	8
12	600	2800	75	6
13	1000	2800	75	7
14	600	2800	100	6
15	1000	2800	100	7

Fig. 3. In models 1–4, the underlap Δ_y is fixed at 2800 m (seed length is 400 m) and the offset Δ_x varies between 600 m and 1200 m. The evolution of the grabens through time is depicted from left to right. For models 1–4, elevation z(m) is shown in top view and in the region marked with a dotted line, a cross-section representing accumulated strain (the red regions are fully strain-weakened, i.e. $\varepsilon > \varepsilon_2$) is shown. The initial position of the weak seeds is indicated in the first panel for each model. On the right, 3D views of models 1 and 3 are shown at t = 350 ka, along with strain rate for the three cross-sections indicated.

(3) With the exception of pre-defined weak seeds at the base of the brittle layer, our models are homogeneous throughout, and thus do not take into account the mechanical anisotropy that is present in the form of densely spaced joint sets in the Canyonlands region. Although the heterogeneity in strength in natural systems undoubtedly influences the nature of graben interaction, our models can allow us to study basic first-order features that result from varying parameters such as graben spacing and thickness of salt layer.

Sensitivity tests

With the following models, we investigate: (1) the influence of the seed offset Δ_x; (2) the influence of the underlap Δ_y (Huggins *et al.*, 1995); and (3) the influence of the salt

layer thickness, h_2. The values of the parameters used for models 1–15 are summarized in Table 2.

RESULTS

Effect of varying seed offset Δ_x

Underlap Δ_y = 2800 m

Models 1–4 (Fig. 3) explore how the offset Δ_x between grabens affects the evolution and interaction of the structures when the distance between the tips of the weak seeds (each of size 400 m), Δ_y, is fixed at 2800 m.

In model 1, the weak seeds are offset by a distance Δ_x = 600 m. Deformation localizes primarily in the weak seed regions, where two strain-weakened conjugate frictional-plastic shears root at an angle of approximately 55º. As extension proceeds, these shears give rise to the formation of two grabens each of width *ca.* 600 m. At t = 150 ka (Fig. 3a), as deformation accumulates in the central region, the outermost plastic shears in both grabens start to curve towards each other. At t = 250 ka (Fig. 3b), further accumulation of strain in the central region causes the grabens to rotate towards the central region, deviating sharply from the original graben trends. The innermost plastic shears that are almost aligned have a self-reinforcing effect on each other and reach strain-weakening values faster than the outermost shears, which are gradually abandoned, forming ramps at both graben ends. The asymmetry resulting from strain focusing preferentially in the innermost shear bands causes the grabens to develop into half-grabens. At t = 350 ka, a thin horst (Fig. 3c) is formed in the overlapping region between grabens as the shears with opposing dip meet. The grabens have each propagated more than halfway through the model domain resulting in a change of polarity in the central region. Minor faults antithetic to the main fault develop in the walls bounding the graben segments that link to the relay ramps.

In model 2 where Δ_x = 800 m, the grabens are initially too far apart to interact and propagate along strike. At t = 150 ka (Fig. 3d), the zones of diffuse deformation from each graben overlap, forming secondary conjugate shear bands in the central region. At t = 250 ka (Fig. 3e), the grabens propagate further and as the secondary shear bands reach strain weakened values, a secondary graben parallel to the primary grabens forms in the central region. At t = 350 ka (Fig. 3f), the secondary graben propagates and links to the two initial primary grabens in a continuous structure. Two relic topographic highs remain from the boundaries between the central secondary graben and the main graben segments. As deformation focuses in the central region, both of the initial grabens terminate in relay ramps.

In model 3, the weak seeds are offset by a distance of 1000 m (Fig. 3g). This model exhibits behaviour that is very similar to model 2. In this case, deformation is slightly more distributed across the system and lateral secondary shear bands appear adjacent to the primary shear bands that develop in the weak seed regions. At t = 250 ka (Fig. 3h), the innermost shear bands curve around the central region which accumulates strain in conjugate secondary shear bands. An oblique secondary graben is formed as strain-weakening values are reached in the central region. The two primary grabens, labelled A and B (Fig. 3i) become increasingly asymmetric as strain focuses preferentially in the innermost shears. The lateral secondary shear bands are no longer active. At t = 350 ka, the secondary graben, labelled C (Fig. 3i) propagates as it rotates slightly to align with the primary grabens. Two distinct relay ramps are formed at each end. The faults bounding the secondary graben are fully strain-weakened and as the material in this region subsides further, two thin horsts around the graben remain.

In model 4, the weak seeds are offset by a distance of 1000 m. At t = 150 ka (Fig. 3j), the grabens formed in the weak seed regions are now too far apart to have a direct influence on each other. Deformation is distributed throughout the system and a secondary conjugate set of shear bands appears at a lateral distance of *ca.* 1800 m from one of the main grabens formed in one of the weak seed regions, and at a distance of *ca.* 600 m from the other weak seed. The proximity of this secondary set of conjugate shear zones and the graben formed in the weak seed region results in more strain accumulation in the region between them than in the central region between the primary grabens. At t = 250 ka (Fig. 3k), both the primary graben and secondary graben have propagated almost half way across the domain. The outermost shear band of the primary graben becomes the main active fault and connects to the innermost shear band of the secondary graben (Fig. 3l). The initial primary graben segment on the right is abandoned as all deformation focuses in the other main graben, which reaches strain weakening values first. As the two active grabens continue propagating alongside each other, a thin horst remains between the two graben structures.

Underlap Δ_y = 1800 m

In models 5–8 (Fig. 4), the distance between the tips of the weak seeds (each of size 900 m) is Δ_y = 1800 m.

In model 5, the weak seeds are offset by a distance of 600 m. Although the model behaviour is very similar to that observed in model 1, deformation now localizes more efficiently in the weak seed region owing to the longer seed. At t = 150 ka (Fig. 4a), both grabens formed in the weak seed regions propagate efficiently. The innermost shears are aligned and have a self-reinforcing effect on each other. At t = 250 ka (Fig. 4b), the innermost shears reach strain weakened values and the grabens propagate along strike. Further propagation causes the innermost shear bands dipping in opposite direction to meet. This results in the formation of a narrow horst between the grabens. At 350 ka (Fig. 4c), the innermost part of the
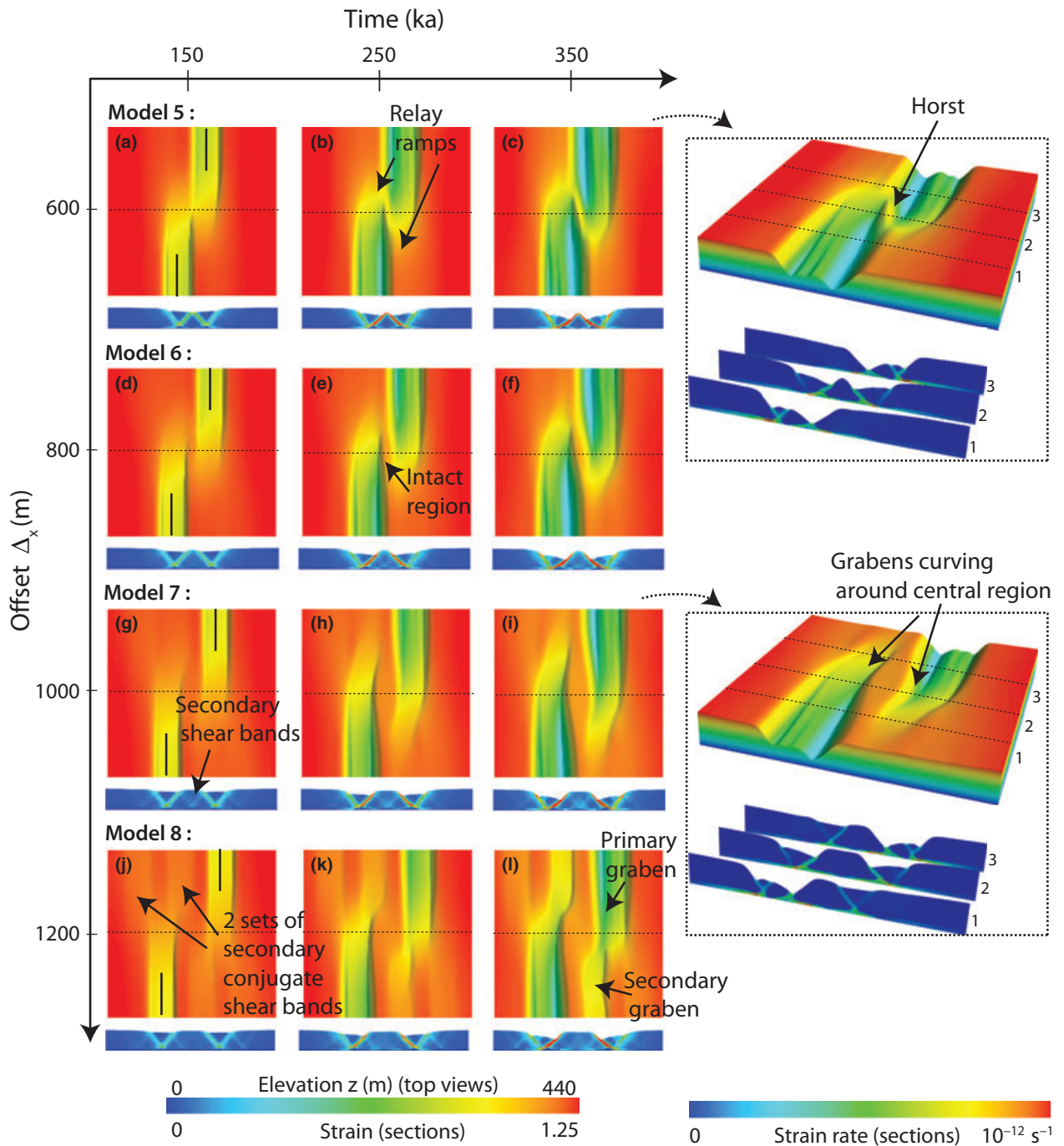
Fig. 4. In models 5–8, the underlap Δ_y is fixed at 1800 m (seed length is 900 m) and the offset Δ_x varies between 600 m and 1200 m. The evolution of the grabens through time is depicted from left to right. For models 5–8, elevation z(m) is shown in top view and in the region marked with a dotted line, a cross-section representing accumulated strain (the red regions are fully strain-weakened, i.e. $\varepsilon > \varepsilon_2$) is shown. The initial position of the weak seeds is indicated in the first panel for each model. On the right, 3D views of models 5 and 7 are shown at t = 350 ka, along with strain rate for the three cross-sections indicated on the figure.

grabens link into a continuous and very well-defined horst structure, and the outermost part of each graben ends in a relay ramp. Further extension leads to widening of the continuous graben structure.

In model 6, the weak seeds are offset by a distance of 800 m. At t = 150 ka (Fig. 4d), the grabens initially propagate along strike independently of each other. As the innermost shear bands accumulate more strain, they become the main active faults and continue to propagate along strike, the grabens become asymmetric. At t = 250 ka (Fig. 4e), each graben has propagated more than halfway across the domain and overlap, leaving a central intact region. The outermost shear bands are gradually abandoned at t = 350 ka (Fig. 4f). The innermost shear bands curve slightly around the overlapping region between the grabens but overall propagation is favoured over linkage.
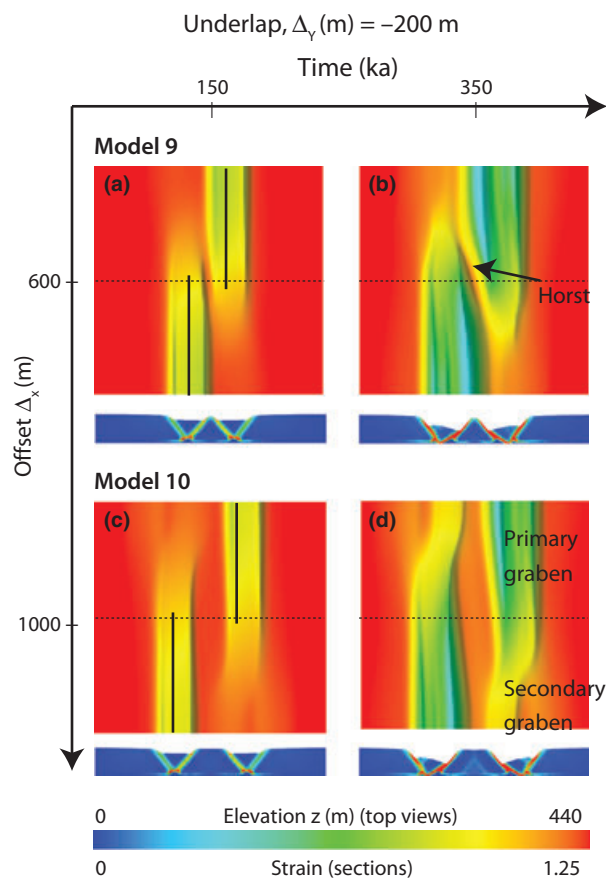
Underlap, Δ_Y (m) = −200 m

Fig. 5. In models 9–10, the underlap is fixed at $\Delta_y = -200$ m (seed length = 1400 m) i.e. the seeds overlap by 100 m and the offsets Δ_x are, respectively, 600 m and 1000 m. For each model, the elevation, z (m) and a cross-section of the accumulated strain is shown at t = 150 ka and t = 350 ka.

In model 7, the weak seeds are offset by a distance of 1000 m. At t = 150 ka (Fig. 4g), as grabens form in the weak seed regions, a secondary set of conjugate shear zones in the central region also appears. At t = 250 ka (Fig. 4h), the grabens curve around the central region and become asymmetric as the innermost shears acquire more strain. The secondary shear bands are abandoned in favour of the innermost shears, which reach strain weakened values first. Subsequently at t = 350 ka (Fig. 4i), the grabens continue to propagate mostly along strike, curving slightly around the central region.

In model 8, the weak seeds are offset by a distance of 1200 m. At t = 150 ka (Fig. 4j), deformation is accommodated not only in the weak seed regions, but also by two sets of secondary conjugate shear bands positioned at regular intervals from the primary grabens. At t = 250 ka (Fig. 4k), as the innermost shear bands acquire more strain and first reach strain weakening values, they propagate faster and start to link up with a set of secondary shear bands across the domain. The outermost shears are abandoned. The innermost shears curve to connect to the secondary shear bands. At t = 350 ka (Fig. 4l), the primary and secondary grabens link up and become the active part of the system. The grabens eventually propagate throughout the system.

Underlap $\Delta_y = -200$ m

In models 9 and 10 (Fig. 5), the distance between the tips of the weak seeds (each of size 1900 m) is $\Delta_y = -200$ m. i.e. the weak seeds overlap for a distance of 100 m.

In model 9, the weak seeds are offset by a distance of 600 m. At t = 150 ka (Fig. 5a), the grabens propagate efficiently along-strike independently of each other. At t = 350 ka, both grabens continue propagating, curving slightly away from each other in an anticlockwise direction, leaving a major horst (Fig. 5b) in the central region.

In model 10, the weak seeds are offset by a distance of 1000 m. At t = 150 ka (Fig. 5c), the grabens propagate efficiently along strike. At t = 350 ka (Fig. 5d), each graben links with the secondary shear bands formed across the domain, thus facilitating propagation throughout the system.

Sensitivity to salt thickness, h_2

Offset $\Delta_x = 600$ m

Models 1, 12 and 14 (Fig. 6) show how varying the thickness of the salt layer, h_2, affects the overall graben structures when the offset $\Delta_x = 600$ m.

As seen in a previous section, model 1 (where $h_2 = 50$ m) is characterized by the presence of a thin horst in the central region (Fig. 6c), which forms as a result of the grabens propagating predominantly along-strike so that the innermost shear bands of opposing polarity meet in an overlapping conjugate divergent transfer zone (Morley *et al.*, 1990). The grabens formed are highly asymmetric.

In model 12, the thickness of the salt layer, h_2 is 75 m. At t = 150 ka (Fig. 6d), the outermost shear bands tend to start curving towards one another at an earlier stage than in model 1. The innermost shear bands from the approaching grabens meet in an overlapping conjugate convergent transfer zone (Morley *et al.*, 1990). At t = 250 ka, the grabens link in an oblique manner into a continuous structure. The basins formed are less asymmetric as the less dense salt rises and compensates for the deeper part of the graben.

In model 14, the thickness of the salt layer, h_2 is 100 m. At t = 150 ka (Fig. 6g), the grabens link even earlier, curve towards one another and connect to form an oblique continuous structure. At t = 250 ka (Fig. 6h), the shear bands bounding the graben reach strain weakened values. At t = 350 ka (Fig. 6i), the salt rises, causing asymmetry in the grabens.

Offset $\Delta_x = 1000$ m

Models 3, 13 and 15 (Fig. 7) show how varying the thickness of the salt layer, h_2, affects the overall structure of the graben structures when the offset $\Delta_x = 1000$ m.

In model 3, the thickness of the salt layer, h_2 is 50 m. Model 3 (e.g., section 4.1.1; Fig. 7a) is characterized by

the formation of a secondary graben in the area between the two primary grabens. Lateral secondary shear bands are abandoned as strain localizes in the central region.

In model 13, the thickness of the salt layer, h_2 is 75 m. At t = 150 ka (Fig. 7d), the grabens formed in the weak seed region, propagate along-strike. A set of conjugate shears forms at a lateral distance of *ca.* 1600 m to the main grabens. The lateral secondary gra–

ben has an offset of *ca.* 600 m with the primary gra–bens on the opposing side of the model domain. At t = 250 ka (Fig. 7e), distributed strain accumulates in three domains: (1) along-strike; (2) in the linkage area between the grabens and (3) in the lateral region to the main graben. The innermost shear bands accumulate slightly more deformation than elsewhere and start to strain weaken first after which the outermost shear
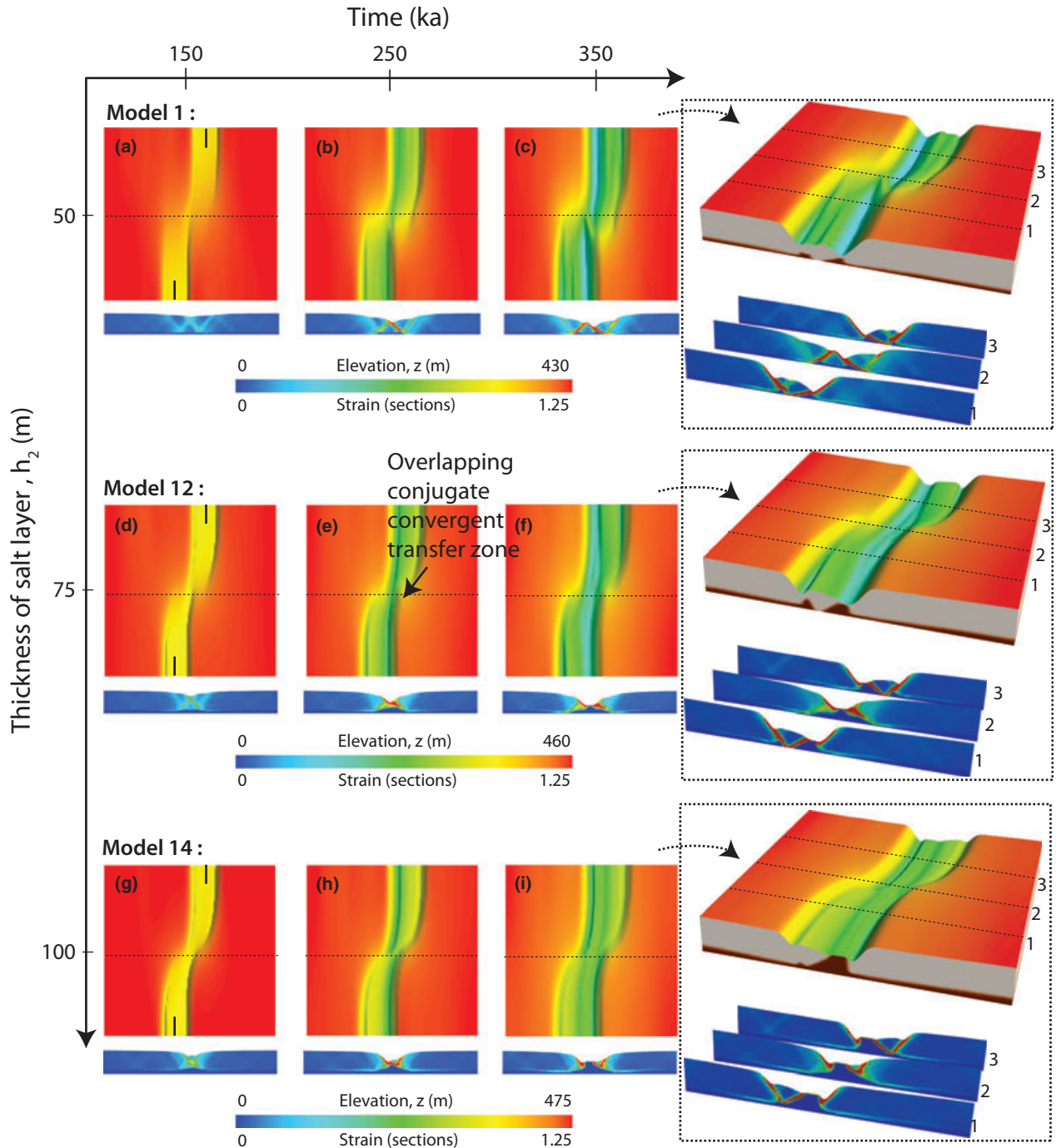

Fig. 6. In models 1, 12 and 14, the offset Δ_x = 600 m and the thickness of the salt layer, h_2 varies between 50 m and 100 m (underlap Δ_y is fixed at 2800 m). The evolution of the grabens through time is depicted from left to right, with top views of elevation z (m) and cross-sections representing accumulated strain (the red regions are fully strain-weakened, i.e. $\varepsilon > \varepsilon2$). The initial position of the weak seeds is indicated in the first panel for each model. On the right, 3D views of the models are shown at t = 350 ka.
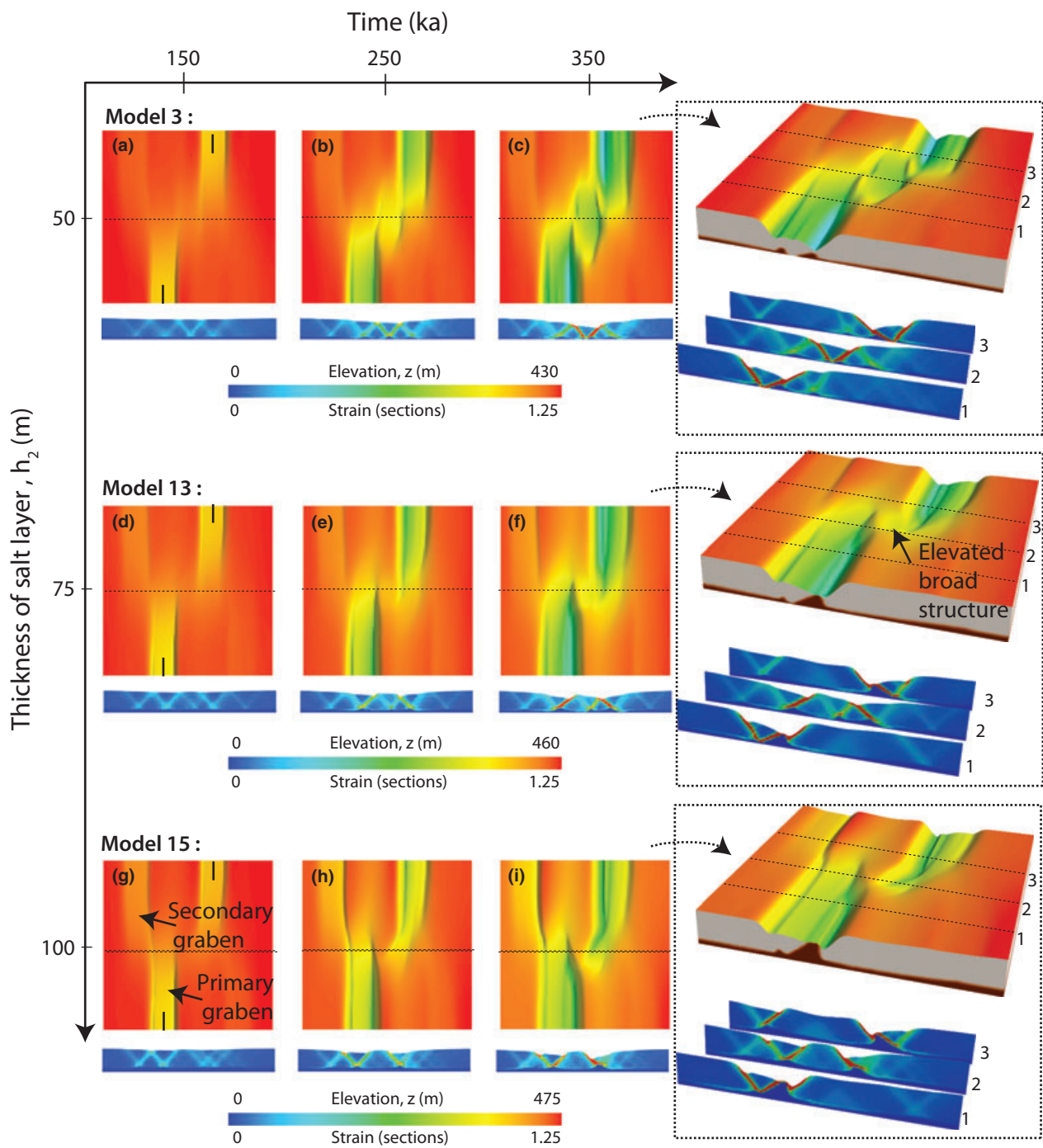
Fig. 7. In models 3, 13 and 15, the offset $\Delta_x = 1000$ m and the thickness of the salt layer, h_2 varies between 50 m and 100 m (Δ_y is fixed at 2800 m). The evolution of the grabens through time is depicted from left to right, with top views of elevation z (m) and cross-sections representing accumulated strain (the red regions are fully strain-weakened, i.e. $\varepsilon > \varepsilon_2$). The initial position of the weak seeds is indicated in the first panel for each model. On the right, 3D views of the models are shown at t = 350 ka.

bands are abandoned. At t = 350 ka (Fig. 7f), the underlying salt layer rises and the innermost shear bands reach strain weakened values. The central region between the primary grabens remains a relatively elevated and broad horst structure.

In model 15, the thickness of the salt layer, h_2 is 100 m. At t = 150 ka (Fig. 7g), the grabens formed in the weak seed region, and the lateral graben localize more effi-

ciently than in models 3 and 13, and consequently propagate faster. At t = 250 ka (Fig. 7h), one of the primary grabens curves towards the central region while the other primary graben links away from the central region, towards the lateral secondary graben across the model domain. At t = 350 ka (Fig. 7i), the secondary lateral graben starts to link with the primary graben while the other graben continues curving towards the central region.
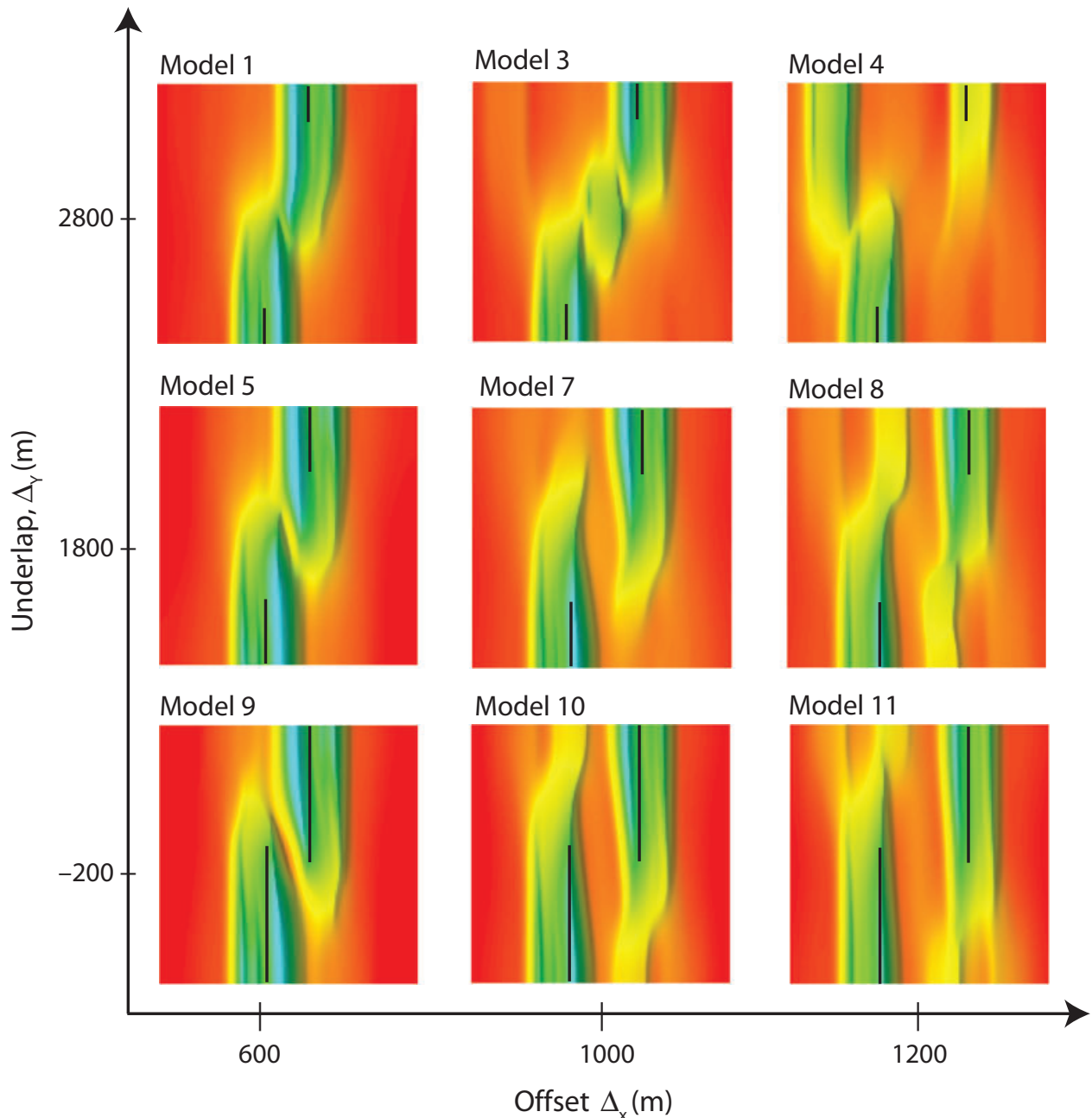
Fig. 8. Summary of model behaviour showing the effect of varying offset Δ_x and underlap Δ_y. All the models are shown at time $t = 350$ ka. The initial position of the weak seeds (which are at the base of the brittle layer, at a depth of 400 m) is indicated with black lines.

DISCUSSION

Although our numerical models are much simpler than natural systems where far more heterogeneity in material properties can be expected, the range of styles they display for varying initial graben spacing compares well with graben structures observed in the Canyonlands area. The numerical models indicate that the spacing between pre-existing weaknesses plays a crucial role in determining the nature of graben interaction. Four distinct types of structures can be observed when the spacing between inherited weakness zones is varied: (1) grabens connecting in a relay zone divided by a narrow central horst; (2) grabens seg-

ments interacting via a secondary step-over graben; (3) grabens propagating alongside each other with limited segment interaction; and (4) an abandoned graben segment in a system of multiple competing grabens (Fig. 8). This diversity of structures can be explained in terms of the efficiency of strain localization and graben linkage. By default, distributed deformation tends to accumulate in the region ahead of the initial weak seeds, causing the grabens to propagate. As the zones of diffuse distributed deformation from both grabens start to overlap, linkage between the grabens through the formation of a secondary intermediate structure may be given precedence over propagation if the central region reaches strain-weakening
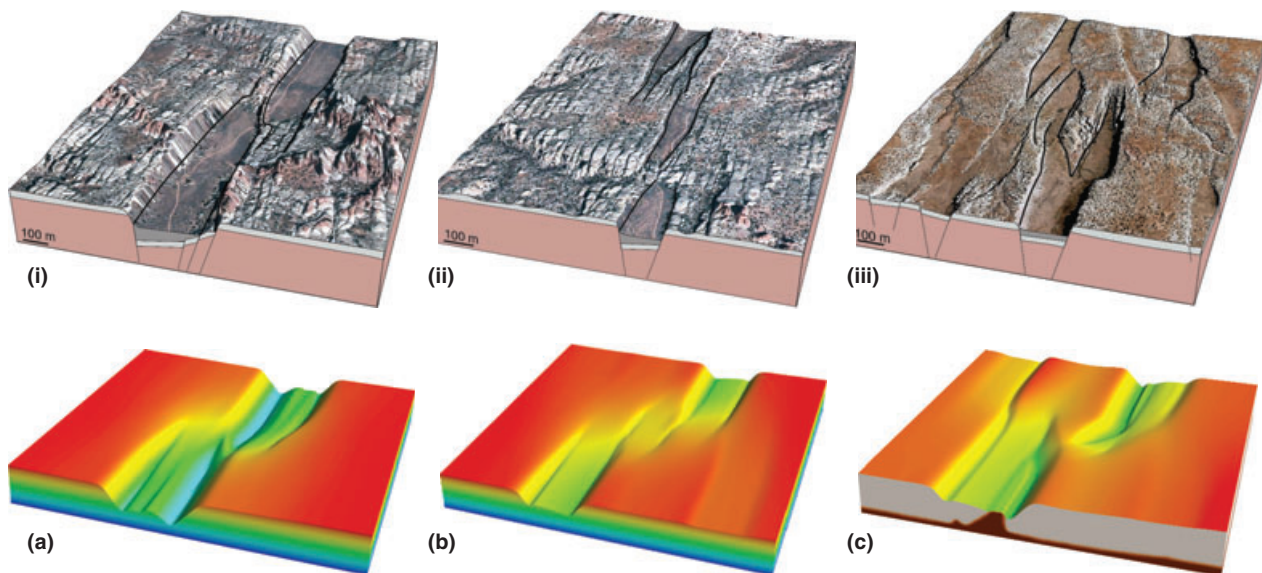
Fig. 9. Selected 3D examples (i, ii, iii) of different styles of graben interaction in the Canyonlands area. The white layer represents an internal sandstone unit in the sedimentary sequence layer within the Cutler formation. Note the densely spaced joint sets that are visible on the surface of the block diagram. Models 1, 3, 15 (a, b, c) shown underneath compare relatively well with the structures observed in that region and can provide an explanation for their formation.

values first. In cases where deformation is more distributed throughout the system, secondary shear bands formed throughout the system may accumulate enough strain to compete with the initial tendency of the main grabens to propagate. The evolution of the system thus depends on the relative efficiency of strain accumulation and resulting localization: (1) along strike; (2) in the linkage area; and (3) in the lateral zones adjacent to main grabens.

Effect of graben spacing and underlap

Small graben offsets (Δ_x) tend to favour linkage between approaching grabens as a result of the self-reinforcing effect caused by the overlap between zones of diffuse deformation from each graben. The horst formed in the overlapping region where shears dipping in opposite directions meet, for small offset grabens (for e.g., in model 1, Fig. 3, 9a) can explain the formation of the narrow horst observed in the Devil's Lane (Fig. 9i). For intermediate offsets, deformation is accommodated in secondary conjugate shear bands in the central region. As strain-weakening values are reached first in this region, linkage of the grabens through a secondary graben is favoured over propagation. These structures can be compared with another part of the Canyonlands (Fig. 9ii), which is characterized by three moderately offset grabens. In this region, the intermediate graben has undergone less extension than the other two grabens, suggesting that it was formed relatively late during the growth history of the primary grabens, as in model 3 (Fig. 3,9b). Beyond a certain critical offset Δ_x, the grabens are too far apart to interact and strain accumulation in the linkage area becomes inefficient. This results in an increase in impor-

tance of secondary shear zones throughout the system, which results in deformation becoming more distributed.

The main effect of increasing the length of the pre-existing weakness zones, i.e., decreasing the distance between the tips of the weak seeds Δ_y, is to increase the efficiency of along-strike propagation as deformation is more localized. The larger strength perturbation owing to the more pronounced pre-existing weakness zone results in more efficient localization and propagation of the graben zone. For larger offsets, as deformation localizes efficiently in the weak seed regions, there is a smaller tendency for secondary shear bands to form adjacent to the grabens. The grabens thus tend to propagate along-strike with reduced interaction with each other. Although lateral secondary shear bands localize more efficiently for large offsets Δ_x, propagation of the main grabens still dominates owing to the higher strength perturbation provided by the initial weak seed regions.

Role of the effective salt detachment layer

Models 12–15 indicate that graben evolution and interaction is highly dependent on the thickness of the underlying salt layer. Isostatic compensation by the salt layer results in more symmetrical grabens. The salt layer facilitates the localization of deformation and keeps deformation in the system localized as the slightest heterogeneity in the brittle layer is emphasized when the less dense salt rises to fill in the space created. This results in more efficient strain weakening both along strike and in lateral zones adjacent to the main grabens. Individual grabens are more localized and link more easily when the salt layer is thicker. Because the viscous salt layer allows for vertical motion of the brittle layer, a thicker salt layer results in a less constrained

system. The grabens evolve more freely and start to curve towards each other at an earlier stage. A thick salt layer thus favours oblique linkage between grabens.

Our model results can give some indication as to the thickness of the effective salt layer in the Canyonlands region, which is not very well constrained. Although in some instances (e.g., model 15, Fig. 9c), models with a thick salt layer give rise to structures that can be compared with specific regions of the Canyonlands (Fig. 9iii), the general structural pattern in Canyonlands are best matched with those modelled with a salt thickness h_2 of 50 m (e.g., Fig. 9i, ii). This suggests that the effective salt detachment in the Canyonlands region is relatively thin compared to the brittle layer. The pervasive asymmetry observed in the cross-sectional form of the grabens (Moore & Schultz, 1999) is also best reproduced with a thin salt layer. This may be explained by the combined effect of strain weakening which favours preferential development of the inner shear zones and the limited amount of isostatic compensation that is allowed by the presence of a thin salt detachment layer.

Comparison with earlier work comprising only a brittle layer (Allken *et al.*, 2011) indicates that even the presence of a thin salt layer makes a significant difference, particularly for large offset grabens. Even though the salt layer is too thin to allow significant rotation of the grabens, it promotes efficient graben propagation and localization of secondary lateral shear bands. This leads to the formation of independent grabens or secondary lateral grabens, depending on the strength of the initial perturbation, and explains why the single-layered models of Allken *et al.* (2011) differ from the structures obtained with a thin salt layer when the graben offset is large.

CONCLUSION

The diversity of structures observed in the Canyonlands region can be explained by the initial spacing and overlap between pre-existing structures. Four distinct types of structures can be observed when the spacing between inherited weakness zones is varied: (1) small-offset grabens connecting in a relay zone divided by a narrow central horst; (2) intermediate-offset grabens segments interacting via a secondary step–over graben for large initial underlaps; (3) intermediate and large offset grabens propagating alongside each other with limited segment interaction for small initial underlaps; and (4) an abandoned graben segment in a system of multiple competing grabens for large offsets and underlaps. We expect the same range of controls to operate at larger scales as well. Linkage at continental crustal scale rift systems may be similarly controlled by offset between individual grabens, the degree of weakening and brittle-ductile coupling (e.g., Allken *et al.*, 2011, 2012). Our results suggest that the salt layer in the Canyonlands region is relatively thin, as the general structural pattern in Canyonlands are best matched with those modelled with an effective salt thickness h_2 of 50 m. This indicates that the system in that region is relatively constrained.

REFERENCES

ALLKEN, V., HUISMANS, R.S. & THIEULOT, C. (2011) Three-dimensional numerical modeling of upper crustal extensional systems. *J. Geophys. Res.*, **116**, B10409. doi:10.1029/2011JB008319.

ALLKEN, V., HUISMANS, R.S. & THIEULOT, C. (2012) Factors controlling the mode of rift interaction in brittle-ductile coupled systems: a 3D numerical study. *Geochem. Geophys. Geosyst.*, **13**, Q05010. doi:10.1029/2012GC004077.

BAKER, A. (1933) *Geology and oil possibilities of the Moab district, Grand and San Juan Counties*. Geological Survey Bulletin, Utah, US. p.841.

BARBEAU, D.L. (2003) A flexural model for the Paradox Basin: implications for the tectonics of the Ancestral Rocky Mountains. *Basin Res.*, **15**(1), 97–115.

BIGGAR, N.E. & ADAMS, J.A. (1987) Dates derived from Quaternary strata in the vicinity of Canyonlands National Park. In: *Geology of Cataract Canyon and Vicinity: Four Corners Geological Society* (Ed. by J.A. Campbell), pp.127–136. Four Corners Geological Society, Durango, CO.

BYERLEE, J. (1978) Friction of rocks. *Pure Appl. Geophys.*, **4–5**, 615–626.

CARTWRIGHT, J.A. & MANSFIELD, C.S. (1998) Lateral displacement variation and lateral tip geometry of normal faults in the Canyonlands National Park, Utah. *J. Struct. Geol.*, **20**(1), 3–19.

CARTWRIGHT, J.A., TRUDGILL, B.D. & MANSFIELD, C.S. (1995) Fault growth by segment linkage - An explanation for scatter in maximum displacement and trace length data from the Canyonlands grabens of SE Utah. *J. Struct. Geol.*, **17**(19), 1319–1326.

COWIE, P.A., GUPTA, S. & DAWERS, N.H. (2000) Implications of fault array evolution for synrift depocentre development: insights from a numerical fault growth model. *Basin Res.*, **12**(3–4), 241–261.

FOSSEN, H., SCHULTZ, R.A., RUNDHOVDE, E., ROTEVATN, A. & BUCKLEY, S.J. (2010) Fault linkage and graben stepovers in the Canyonlands (Utah) and the North Sea Viking Graben, with implications for hydrocarbon migration and accumulation. *AAPG Bull.*, **94**(5), 597–613.

FURUYA, M., MUELLER, K. & WAHR, J. (2007) Active salt tectonics in the Needles District, Canyonlands (Utah) as detected by interferometric synthetic aperture radar and point target analysis: 1992-2002. *J. Geophys. Res.*, **112**, 18 pp.

HUGGINS, P., WATTERSON, J., WALSH, J.J. & CHILDS, C. (1995) Relay zone geometry and displacement transfer between normal faults recorded in coal-mine plans. *J. Struct. Geol.*, **17** (12), 1741–1755.

HUNTOON, P.W. (1982) The Meander anticline, Canyonlands, Utah: An unloading structure resulting from horizontal gliding on salt. *Geol. Soc. Am. Bull.*, **93**, 941–950.

JACKSON, C.A.L., GAWTHORPE, R.L. & SHARP, I.R. (2002) Growth and linkage of the East Tanka fault zone, Suez rift: structural style and syn-rift stratigraphic response. *J. Geol. Soc.*, **159**, 175–187.

KAUS, B. (2010) Factors that control the angle of shear bands in geodynamic numerical models of brittle deformation. *Tectonophysics*, **484**(1–4), 36–47. doi:10.1016/j.tecto.2009.08.042.

McGILL, G.E. & STROMQUIST, A.W. (1979) Grabens of Canyonlands National Park, Utah: Geometry, Mechanics, and Kinematics. *J. Geophys. Res.*, **84**(NB9), 4547–4563.

McGILL, G.E., SCHULTZ, R.A. & MOORE, J.M. (2000) Fault growth by segment linkage: an explanation for scatter in maximum displacement and trace length data from the Canyonlands grabens of SE Utah: Discussion. *J. Struct. Geol.*, **22**(1), 135–140.

MELOSH, H.J. & WILLIAM, C.A. (1989) Mechanics of graben formation in crustal rocks: A Finite Element analysis. *J. Geophys. Res.*, **94**(B10), 13961–13973.

MOORE, J.M. & SCHULTZ, R.A. (1999) Processes of faulting in jointed rocks of Canyonlands National Park, Utah. *Geol. Soc. Am. Bull.*, **111**(6), 808–822.

MOREWOOD, N.C. & ROBERTS, G.P. (2002) Surface observations of active normal fault propagation: implications for growth. *J. Geol. Soc.*, **159**, 263–272.

MORLEY, C.K. (1999) How successful are analogue models in addressing the influence of pre-existing fabrics on rift structure? *J. Struct. Geol.*, **21**(8–9), 1267–1274.

MORLEY, C.K., NELSON, R.A., PATTON, T.L. & MUNN, S.G. (1990) Transfer zones in the East-African rift system and their relevance to hydrocarbon exploration in rifts. *AAPG Bull.*, **74**(8), 1234–1253.

RANALLI, G. (1995) *Rheology of the Earth*. Chapman and Hall, London, UK.

SCHULTZ-ELA, D.D. & WALSH, P. (2002) Modeling of grabens extending above evaporites in Canyonlands National Park, Utah. *J. Struct. Geol.*, **24**(2), 247–275.

THIEULOT, C. (2011) FANTOM: two- and three-dimensional numerical modelling of creeping flows for the solution of geological problems. *Phys. Earth Planet. Inter.*, **188**, 47–68.

TRUDGILL, B.D. (2002) Structural controls on drainage development in the Canyonlands grabens of southeast Utah. *AAPG Bull.*, **86**(6), 1095–1112.

TRUDGILL, B.D. (2011) Evolution of salt structures in the northern Paradox Basin: controls on evaporite deposition, salt wall growth and supra-salt stratigraphic architecture. *Basin Res.*, **23**(2), 208–238.

TRUDGILL, B. & CARTWRIGHT, J. (1994) Relay-ramp forms and normal-fault linkages, Canyonlands National Park, Utah. *Geol. Soc. Am. Bull.*, **106**(9), 1143–1157.

WALSH, P. & SCHULTZ-ELA, D.D. (2003) Mechanics of graben evolution in Canyonlands National Park, Utah. *Geol. Soc. Am. Bull.*, **115**(3), 259–270.